DOI: 10.24996/ijs.2026.67.3.3

ISSN: 0067-2904

Spectral Studies, Corrosion Inhibition, and *In Vitro* Biological Investigations of Novel Synthesized Metal Complexes of (Rh^{+3}, Pd^{+2}, Pt^{+4}, Au^{+3}) with Acyclovir

Farah Saadoun[1*], Mahasen Faisal[2]

[1]*Ibn Sina University of Medical and Pharmaceutical Sciences, Baghdad, Iraq.*
[2]*Department of Chemistry, College of Science for Women, University of Baghdad. Iraq.*

Received: 1/10/2024 Accepted: 29/3/2025 Published: 30/3/2026

Abstract

The current study describes the synthesis of new complexes of Acyclovir ligand (AL) with heavy metal ions (Rh^{+3}, Pd^{+2}, Pt^{+4}, and Au^{+3}). These complexes were characterized by different analyses techniques, including ^{1}H, ^{13}C-NMR, Mass-spectra, FTIR, UV-Vis., Elemental (CHN) analysis, Flame atomic absorption spectroscopy (FAAS), the Molar conductivity, Magnetic susceptibility, and melting point measurements. The (Metal: Ligand) and Gibbs free energy for all synthesized complexes were determined by the Molar ratio method. The results of all analyses and measurement techniques gave square planar and octahedral geometries for Pd^{+2}, Au^{+3}, and Rh^{+3}, Pt^{+4}, respectively. All complexes are formed in the ratio of (1M: 2L). Acyclovir and some of its complexes behaved as inhibitors against the corrosion of carbon steel in a saline solution of NaCl (3.5%). The results showed that ligand and its complexes are effective and exhibit inhibition efficiency (IE) above 90%. On the other hand, the antibiofilm, antioxidant, and antiproliferative bioactivities of acyclovir and its complexes were investigated. The Rh(III)-complex showed the highest percentage in preventing the biofilm formation of *Escherichia coli* (*E-Coli*) at a low concentration of about 32µg/ml. In contrast, the other complexes and ligand need higher concentrations to exhibit their activity. In addition, the Rh(III)-complex showed the highest percentage in 2,2-diphenyl-1-picrylhydrazyl radical (DPPH) scavenging, followed by AL and Pt-AL. The antiproliferative activity was done versus the HFFs cancer cell line, and the Au^{3+}-complex showed the ability to decrease the viability to about 68.27%.

Keywords: Acyclovir ligand, Anticorrosive, Bioassay, *E coli*, HFFs cell line.

الدراسات الطيفية، تثبيط التآكل والتحقيقات البيولوجية المختبرية للمعقدات المعدنية المحضرة الجديدة مع الاسايكلوفير(Rh^{+3}, Pd^{+2}, Pt^{+4}, Au^{+3})

فرح سعدون[1*] ، محاسن فيصل[2]

[1]جامعة ابن سينا للعلوم الطبية و الصيدلانية, بغداد, العراق

[2]قسم الكيمياء, كلية العلوم للبنات, جامعة بغداد, بغداد, العراق

الخلاصة

تصف الدراسة الحالية تحضير اربع معقدات جديدة من ليكاند الاسايكلوفير مع ايونات العناصر الثقيلة (Rh^{+3}, Pd^{+2}, Pt^{+4}, Au^{+3}). هذه المعقدات شخصت بواسطه عدة تحاليل و تقنيات و التي تضمنت :

*Email: fsjakam@gmail.com

طيف الرنين النووي المغناطيسي و طيف الكتلة و طيف الاشعة تحت الحمراء و مطيافية الأشعة فوق البنفسجية والمرئية و تحليل العناصر (CHN) و الفلزات و قياس التوصيلية الكهربائية و الحساسية المغناطيسية و درجة الانصهار. نسبة الفلز الى الليكاند و ثابت الاستقرار و طاقة غيبس الحرة لجميع المعقدات المحضرة تم تعيينها بواسطة طريقة النسبة المولارية. أسفرت نتائج هذه التحليلات عن اقتراح الاشكال الهندسية المربع المستوي وسداسي السطوح لـ Pd^{+2}, Au^{+3} وRh^{+3}, Pt^{+4} على التوالي. جميع المعقدات مستقرة و تكونت عند النسبة (1فلز : 2 ليكاند). تم تطبيق الاسايكلوفير و بعض معقداته كمثبط لتأكل الفولاذ الكاربوني في وسط ملحي من كلوريد الصوديوم 3,5% , اظهر الاختبار ان جميع المركبات المستخدمة فعالة و تظهر كفاءة تثبيط اكثر من 90% . من ناحية اخرى , تم دراسة الفعالية الحيوية للأسايكلوفير ومعقداته كمضادات للأغشية الحيوية ومضادات الأكسدة ومضادات لتكاثرالخلايا السرطانية. أظهر معقد Rh(III) أعلى نسبة في منع تكوين الأغشية الحيوية في الإشريكية القولونية بتركيز منخفض حوالي 32 ميكروغرام/مل. وفي المقابل تحتاج المركبات الأخرى إلى تركيزات أعلى حتى تظهر نشاطها. أيضًا، يظهر معقد Rh(III) أعلى نسبة في اقتناص DPPH يليه AL وPt–AL. تم إجراء النشاط المضاد للتكاثر مقابل خط الخلايا السرطانية HFFs، واظهر معقد Au^{3+} القدرة على تقليل النمو إلى 68.27%.

1. Introduction

Antiviral therapy has advanced significantly with the discovery of acyclovir, proving that knowledge of molecular interactions can result in efficient treatments for viral infections [1]. Acyclovir is a potent antiviral drug, generally prescribed for the treatment of illnesses caused by specific types of viruses [2]. Most frequently, it is recommended for infections brought on by the varicella-zoster virus (VZV) [3] and the herpes simplex virus (HSV)[4]. Because of its affinity for the enzyme thymidine kinase, which is encoded by HSV and VZV, acyclovir can be thought of as a prodrug. It is delivered in an inactive form and is transformed into two phosphorylated forms [5].

Acyclovir (9-[(2-Hydroxyethoxy)methyl] guanine) is a synthetic nucleoside analogous that is generated from guanine and has an additional acyclic side chain. Chemically, it is classified as a heterocyclic molecule [6]. The chemical structure of acyclovir (aromaticity and presence of active heteroatoms) supports its ability to behave as a chelating agent with metal ions. As is known, transition metal complexes are the most often utilized chemotherapeutic drugs [7], making significant contributions to medical treatments. These complexes have a wide range of actions, including antimicrobials, anti-inflammatories, antiviral, antitumor, antidiabetic, and others [7]. Therefore, one of the ways to improve the properties of some drugs is by introducing metal ions into their composition, either in the form of organometallic compounds or metal complexes [8].

Many previous research studies have used acyclovir as a ligand to form various complexes of biological interest; for example, different forms of Cu^{2+}-ACV complexes have been synthesized and tested their antiviral activity by Boris *et al.,* [9], Panteva *et al.*, [10], and María del *et al*., [11]. Likewise, cis-Platinum (II) analogues based on acyclovir were prepared by Sinur and Grabner [12], Coluccia *et al.,* [13], Balcarová *et al.,* [14], and cis-$[PdCl_2(H_2O)(N7\text{-}ACV)]$ ACV.$2H_2O$ has been prepared by Gómez-Segura *et al.,* [15], all of which have been investigated as antiviral and anticancer. Other metal complexes have been synthesized in different molar ratios of (ACV. : M), and diverse binding sites involved the ions (Cr^{3+}, Mn^{2+}, Fe^{3+}, Co^{2+}, Ni^{2+}, Zn^{2+}, Ru^{3+}, Cd^{2+}, Pt^{2+}, and Hg^{2+}). Some of them have been applied in new fields like DNA cleavage, DNA binding, and antimicrobial studies [16-19]. This study aimed to synthesize new mononuclear complexes by reacting 2 molecules of acyclovir with (Rh^{+3}, Pd^{+2}, Pt^{+4}, Au^{+3}) metal ions and functionalized these complexes in

various uses industrially as (anticorrosive, and antibiofilm) and medically as (antioxidant and antiproliferative of cancer cells).

2-Experimental

2.1-Materials and Instruments

Metal chloride salts (analytical grade) were purchased from Merck (Schnelldorf, Germany), acyclovir powder (99.45%) from Bide Pharmatech Ltd. (China), NaCl (99.5%) from Loba Chemie Pvt. Ltd. (Mumbai, India), and solvents from Alpha Chemika (Mumbai, India). The electronic spectra of compounds in ethanol were measured in the range (200-900) nm by using UV-1800 Shimadzu Spectrophotometer, whereas used FT-IR 8400 Shimadzu spectrophotometer to measure the FTIR spectra in the range (4000-200) cm^{-1} by using disc of CsI. The elemental analysis was performed using an Eager 300 elemental analyzer, and metal content was determined by an AA-6880 Shimadzu atomic absorption spectrophotometer. The conductivity measurements were carried out on PL-700PC meter, GOnDO Electronic Company. The Sherwood scientific magnetic susceptibility instrument was used to obtain the μ_{eff} measures. Additional information about the chemical structure of complexes were gained by Bruker NMR analyzer and mass spectrometer. The corrosion tests were performed using Potentiostat MLab200, Bank Elect. To obtain the images from scanning electron microscope (SEM) analysis, the TESCAN VEGA (III) SEM instrument was used.

2.2-Synthesis of Solid Metal Complexes

To synthesize metal complexes, (2 mmole, 0.45042g) of Acyclovir (AL) were dissolved in 20 ml of absolute ethanol and mixed with 1mmole of (0.209g $RhCl_3$,0.177 g $PdCl_2$, 0.518 g $H_2PtCl_6.6H_2O$ and 0.411 g $HAuCl_4.H_2O$) separately, then refluxed for 3 hrs. Colour changes was observed, and the formation of the precipitates. Then, ethanol was evaporated in the air, and the resulting-coloured complexes were washed several times with petroleum ether and left to dry [18,19]. The physicochemical properties of complexes are listed in Table 1.

2.3- Molar Ratio Method of Complexes in Solution

To verify the formation of complexes at molar ratio = 1M:2AL and calculate the stability constant of each complex, the Molar ratio method is applied. The method involves the addition of varying volumes (0.25-5) ml of 10^{-3}M of ethanolic solution of AL to the constant volume 1 m1 of 10^{-3}M of ethanolic solution of metal salt [$RhCl_3$, $PdCl_2$, $H_2PtCl_6.6H_2O$, and $HAuCl_4.H_2O$] in a volumetric flask (10 ml). The absorbance measurements were obtained at λ_{max} for each complex and plotted against the volume of a stock standard solution of chelator (AL) [20].

2.4- The Measurements of Corrosion

Potentiodynamic polarization tests were conducted on carbon steel (20L×20W×1.5H) mm in blank solution followed by the addition of inhibitor using three different concentrations (20, 60, 80) ppm of tested compounds (AL, Pt^{4+}–AL, Au^{3+}–AL) in a 3.5 % (w/v) NaCl solution at 25°C. The potentiostatic polarization measurements were obtained in open-circuit potential (OCP) by varying the electrode potential between ±200 mV with a constant scan rate of about 3 $mV.s^{-1}$[21].

2.5- Biofilm Inhibition Assay

The inhibition of biofilm formation of acyclovir and their complexes versus clinical isolate of *E. coli* were evaluated using the microtitration plate's method and according to sub-MIC in (μg/ml) for each tested compound which was determined previously by Broth microdilution method, as described by Wang *et al.,* [22]. To examine the efficiency of selected compounds as antibiofilm, the following steps were applied: 1) The sterilized Brain Heart Infusion (BHI) broth was prepared by inoculating the *E. coli* isolates in 5 mL of BHI

supplemented with 2% (w/v) of sucrose, and incubated for 24 hours at 37°C. 2) For each one of the inhibitors to be tested (acyclovir and its complexes), 100 µL of inhibitor at sub-MIC was mixed with 80 µL of the prepared broth and transferred this mixture to a 96-well microplate and followed by the addition of 20 µL of *E. coli* suspension. 3) To prepare the control, 180 µL of broth was mixed with 20 µL of *E. coli* suspension without any addition of inhibitor. 4) The 96-well microplates were incubated overnight at 37°C, then the aliquot was removed, and the wells were washed with sterile phosphate-buffered saline (PBS) to ensure that all non-adherent bacteria were discarded and dried at room temperature for 15 minutes. 5) A 200µL of 0.1% (w/v) of crystal violet was added to the wells and left for 20 minutes to stain the formed biofilm in the bottom of the wells. 6) The stained wells were washed three times with the same washing solution (PBS) at pH equal to 7.2 to remove the unbound dye and left to dry for 15 min. at RT. 7). The last step included the addition of 200 µL of ethanol (95% v/v) to the wells and used the Eliza reader to read the absorbance at 630 nm. The percentage of biofilm formation inhibition was calculated according to equation 1.

$$I\% = \frac{Abs.(control) - Abs.(inhibitor)}{Abs.(control)} \times 100 \quad . \ . \ . \qquad \text{Eq (1)}$$

2.6- Antioxidant Activity Assay

The ability to scavenge free radicals was screened for acyclovir and its four prepared complexes using the DPPH method according to the reference [23]. To prepare 0.1mM of 2,2-diphenyl-1-picrylhydrazyl (DPPH) that was used as a reagent in this method, 4 mg of reagent was dissolved in 100 mL of methanol and stored in a dry and cool place for later use. The stock solution at conc.= 400 µg/mL of the tested sample was prepared by dissolving 4mg of (AL or one of the complexes, individually) in 10 mL of methanol, which was subsequently used to produce a serial dilution with methanol to obtain wanted concentrations [12.5, 25, 50,100, and 200] µg/mL. The reaction was performed by mixing 3mL of the reagent with 2mL of the examined sample in a test tube (once for each concentration) and keeping the mixture in a dark place at 25°C for ½ hour, after that the measurement of the absorbance of the mixture was determined at 517 nm and compared with ascorbic acid as a standard antioxidant. The DPPH inhibition % was calculated according to equation 2.

$$Scavenging\% = \frac{Abs.(blank) - Abs.(sample)}{Abs.(blank)} \times 100 \quad . \ . \ . \qquad \text{Eq (2)}$$

2.7- Antiproliferative Activity Assay

The antiproliferative activity of acyclovir and its complexes of (Pt^{4+} and Au^{3+}) was assessed by the 3-(4,5-dimethylthiazol-2-yl) 2,5-diphenyl tetrazolium bromide (MTT) method [24] against human foreskin fibroblasts (HFFs) cancer cell lines. The viability of cells was determined after being exposed separately to the compounds to be tested at varying concentrations [12.5, 25, 50,100, 200, and 400] µg/mL for 72 hours and compared to the negative control culture value. Compound cytotoxicity was expressed as the IC_{50} value. The optical densities were obtained at 540 nm.

3- Results and Discussions

3.1- Solid and Liquid State of Metal Complexes

The complexes were prepared from acyclovir at a molar ratio = 1M:2AL, which are stable in air, diamagnetic, electrolyte in DMSO, and show good solubility in DMSO, DMF, and relative solubility in polar solvents (dis.H_2O, Abs. ethanol, and methanol). All collected physicochemical properties of complexes are summarized in Table 1.

Table 1: Characteristics of the prepared complexes with Acyclovir Ligand (AL)

Chemical / Molecular formula	Color	Yield %	M.wt g/mol	m.p °C	Conductivity µs.cm^{-1}	Elemental analysis% Found (Calc.)			
						C	H	N	Metal
$[Rh(AL)_2Cl_2]Cl.EtOH$ $C_{18}H_{28}N_{10}O_7Cl_3Rh$	Brown	89	705.74	224d*	65 1:1Electrolyte	38.06 (37.80)	3.92 (4.60)	15.62 (15.43)	------ (15.91)
$[Pd(AL)_2]Cl_2.EtOH$ $C_{18}H_{28}N_{10}O_7Cl_2Pd$	Brown	87	673.80	236	158 1:2 Electrolyte	31.89 (32.05)	4.30 (4.15)	21.47 (20.77)	16.04 (15.79)
$[Pt(AL)_2Cl_2]Cl_2.EtOH$ $C_{18}H_{28}N_{10}O_7Cl_4Pt$	Orangish brown	85	833.37	194-198	180 1:2 Electrolyte	25.58 (25.94)	3.55 (3.39)	16.69 (16.81)	24.03 (23.41)
$[Au(AL)_2]Cl_3.H_2O$ $C_{16}H_{24}N_{10}O_7Cl_3Au$	Yellowish orange	91	771.75	180-182	211 1:3 Electrolyte	25.32 (24.90)	3.07 (3.13)	18.50 (18.15)	25.19 (25.52)

***d = decomposition**

The complexes show high stability in solution. The stability constants, thermodynamic coefficients, and molar absorptivity values for each one of the complexes are shown in Table 2. Whereas the molar ratio plots are displayed in Figure 1. Equations (3–5) were used to calculate the stability constants (K), and according to the values of K, Gibbs free energies (ΔG) can be obtained by applying equation 6 [25]. The results exhibited that the Pt(IV) complex is more stable than others, and all complexes can form spontaneously.

$$A_m = \varepsilon_{max}\, b\, C \quad . \ . \ . \qquad \text{Eq (3)}$$

$$\alpha = \frac{A_m - A_s}{A_m} \quad . \ . \ . \qquad \text{Eq (4)}$$

$$K = \frac{(1-\alpha)}{4\alpha^3\, C^2} \quad . \ . \ . \qquad \text{Eq (5)}$$

$$\Delta G = -RT\, LnK \quad . \ . \ . \qquad \text{Eq (6)}$$

Where:
As: The reading absorbance of the synthesized solution at the ratio (1M:1L)
Am: The reading absorbance of the synthesized solution at the ratio (1M:5L)
C: Molar concentration in Mole.L^{-1}
R: Gas's constant = 8.31 J. K^{-1}.mole^{-1}
T: Temperature in Kelvin = 298 K

Table 2: Show the values of stability constant and Gibbs free energy for each complex.

Complex	As	Am	α	ε_{max} L. mol^{-1}.cm^{-1}	K L^2.mol^{-2}	λ_{max} nm	lnK	ΔG x10^{-3} KJ mol^{-1}
Rh-AL	0.456	1.571	0.709	15710	2.041×10^5	324	12.22	-30.277
Pd-AL	0.032	0.167	0.808	1670	9.099×10^4	381	11.41	-28.276
Pt-AL	0.227	0.353	0.356	3530	3.568×10^6	362	15.08	-37.362
Au-AL	0.068	0.148	0.540	1480	7.303×10^5	418	13.50	-33.434

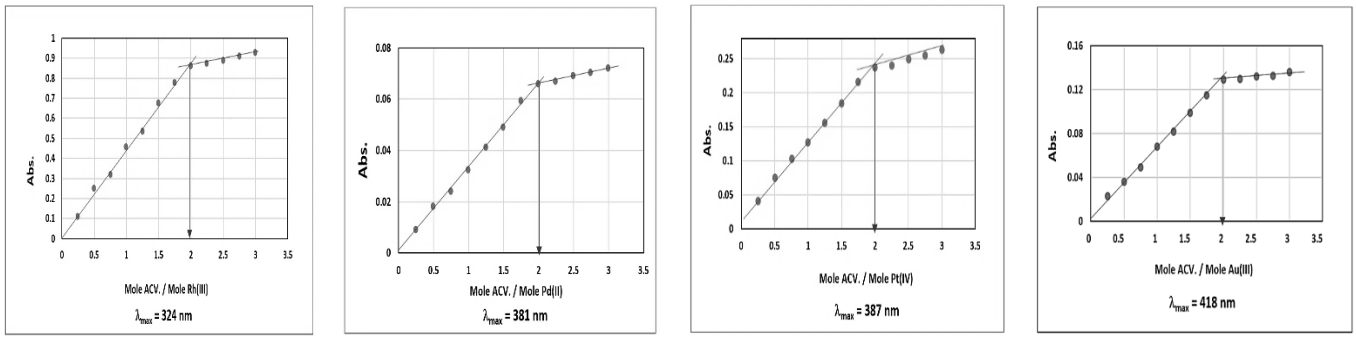

A **B** **C** **D**

Figure 1: Molar ratio for: A) Rh^{3+}–AL , B) Pd^{2+}–AL, C) Pt^{4+}–AL, D) Au^{3+}–AL.

3.2- FT-IR spectra of Acyclovir and Its Metal

The FT-IR spectra of acyclovir and its metal complexes have been examined and assigned in order to elucidate the bonding mode and the impact of the metal ions on the ligand. Here, the bands with the most relevant characteristics are discussed, and all are listed in Table 3 and shown in Figures (2-6).

The spectrum of free ligand (AL) displayed the distinctive bands that absorbed in the region 3440, (3299 and 3193), and 3099 cm^{-1} are attributed to stretching vibration of alcoholic hydroxyl group, asymmetrical and symmetrical stretching of the primary amine group, and νNH of amide, respectively. In addition to the bands of ν(C=O) at 1716 cm^{-1}, ν(N^7=C^8) at 1631 cm^{-1}, bending NH of secondary amide at 1541 cm^{-1}, and ν(CNC) at 1105 cm^{-1} [18,26]. Both carbonyl and imine (C^8=N^7) groups were shifted strongly to lower or higher frequencies confirming the coordination behaviour of acyclovir as O^6, N^7-bidentate ligand. Also, the value of ν(CNC) in all complexes is increased to become between (1120-1108) cm^{-1} [19]. The new bands exhibit at the positions (551-549) cm^{-1}, (499-464) cm^{-1}, and (333-327) cm^{-1} that ascribed to ν(M-O), ν(M-N), and ν(M-Cl) in respective [15,19]. The stretching bands of alcohol were appeared as more intense in (Rh^{+3}, Pd^{+2}, Pt^{+4}) complexes, which may due to the presence of ethanol molecules in the out-sphere of coordinated complexes. Whereas the Au^{+3}-AL complex shows the band at about 3590 cm^{-1} which corresponds to a hydrated water molecule [26].

Table 3: The FTIR data of acyclovir and its metal complexes

Compds	ν(OH)	ν(NH_2)	ν(NH)	ν(C=O)	δ(NH)	ν(C_8=N_7)	ν(M-O)	ν(M-N)	ν(M-Cl)
AL	3440 (Alcohol)	3299 3193	3099	1716	1541	1631	–	–	–
Rh-AL	3674 (Ethanol) 3438 (Alcohol)	3240 3193	3095	1697	1541	1649 1629	550	499	333
Pd-AL	3741 (Ethanol) 3436 (Alcohol)	3305 3184	3091	1697	1539	1619	549	487	-
Pt-AL	3739 (Ethanol) 3446 (Alcohol)	3297 3195	3097	1701	1542	1652 1633	551	487	327
Au-AL	3590 (Hydrated H_2O) 3440 (Alcohol)	3242 3195	3097	1730 1701	1539	1618	549	482	-

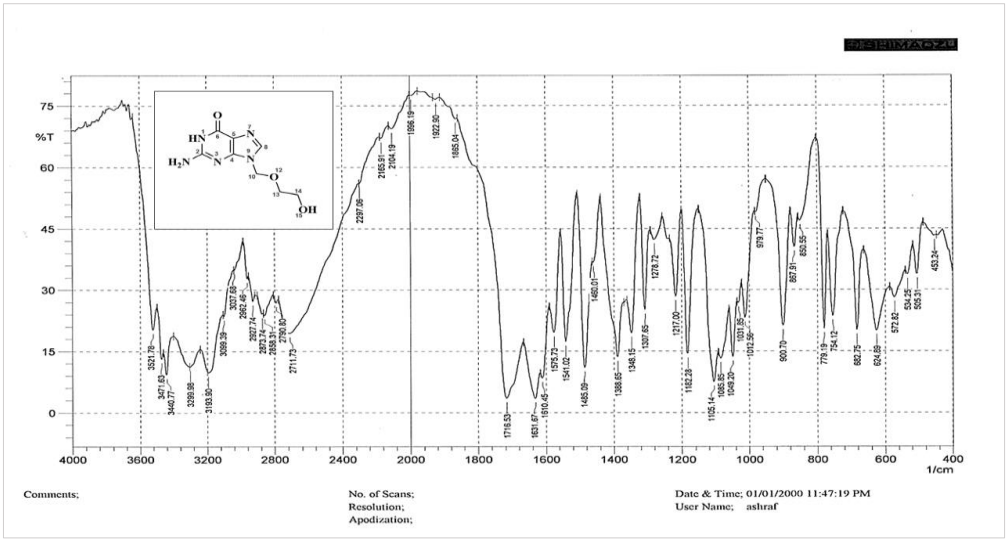

Figure 2: FTIR spectrum of free Acyclovir ligand (AL)

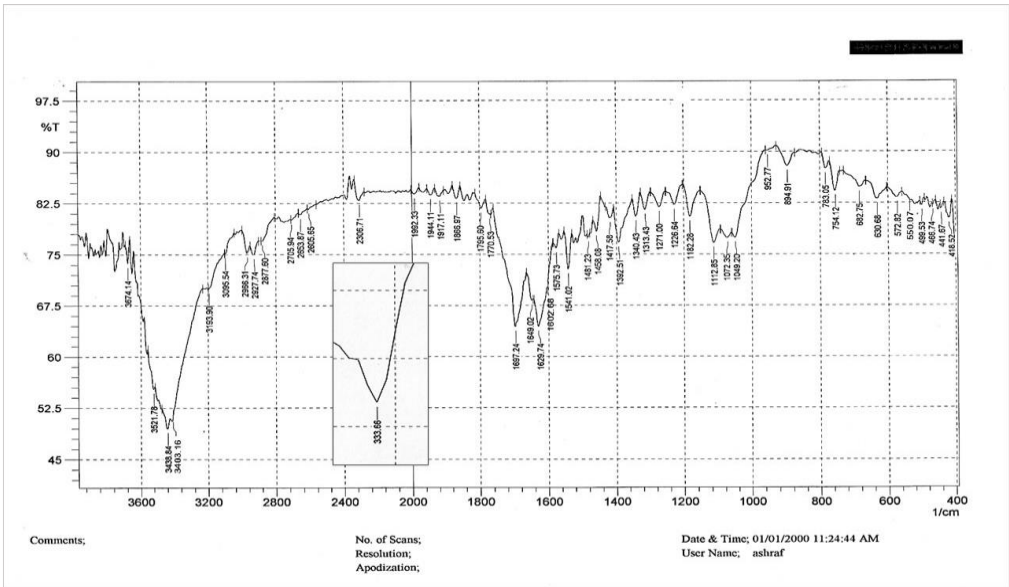

Figure 3: FTIR spectrum of $[Rh(AL)_2Cl_2]Cl$. EtOH complex

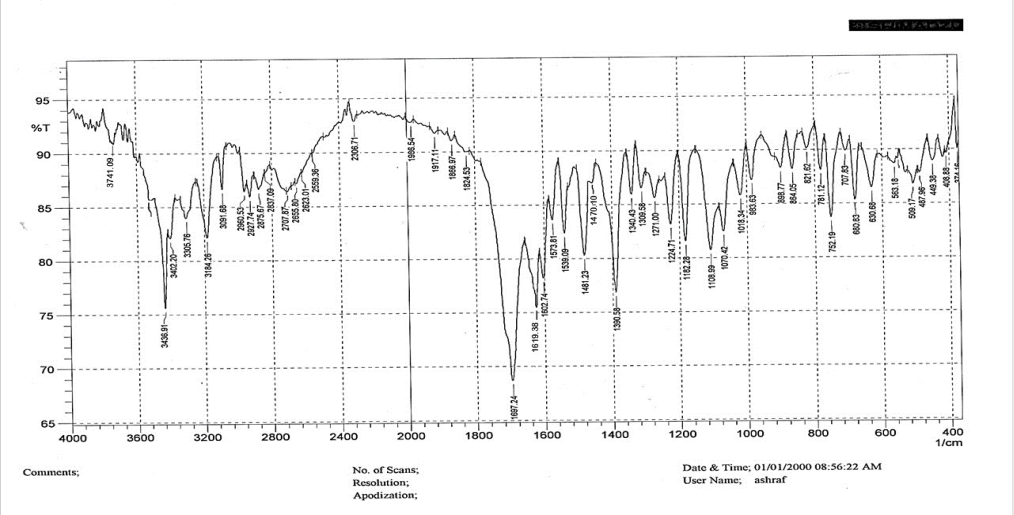

Figure 4: FTIR spectrum of $[Pd(AL)_2]Cl_2$.EtOH complex

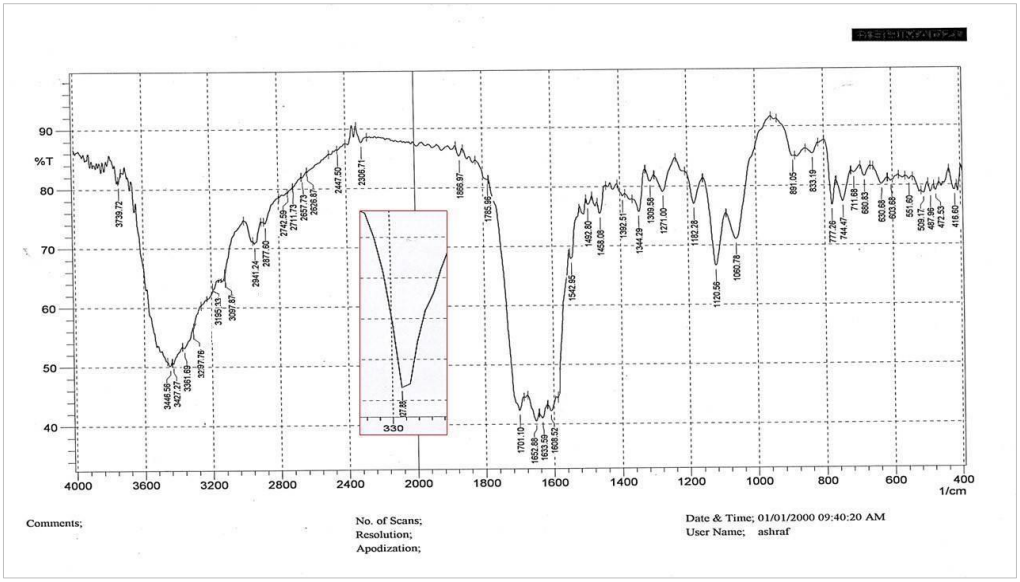

Figure 5: FTIR spectrum of $[Pt(AL)_2Cl_2]Cl_2.EtOH$ complex

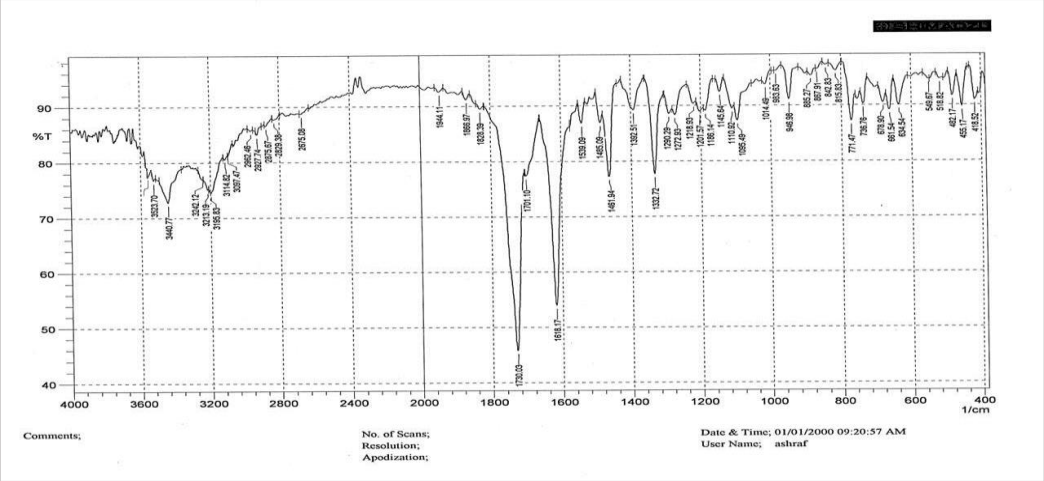

Figure 6: FTIR spectrum of $[Au(AL)_2]Cl_3.EtOH$ complex

3.3-Electronic Spectra of Acyclovir and Its Complexes

The electronic spectra were used to support the proposed geometry of prepared complexes by knowing the electronic transition of each of them. The analysis was performed in ethanolic solutions of all compounds at room temperature in the domain of wavelengths (200-900) nm.

The electronic spectrum of the acyclovir ligand, Figure 7, displayed four maximum peaks as follows: the transition belongs to $\pi\rightarrow\pi^*$ at 205 nm (48780 cm^{-1}) created from the alkene group, whereas the carbonyl group exhibited two transitions as $\pi\rightarrow\pi^*$ at 253 nm (39525 cm^{-1}) and $n\rightarrow\pi^*$ at 272 nm (36764 cm^{-1}), and the fourth is very low-intensity transition at 350 nm (28571 cm^{-1}) assigned to $n\rightarrow\pi^*$ transitions occurred by imine groups [27].

The electronic spectra of the brown Rh^{3+}-AL complex and orangish brown Pt^{4+}-AL complex, Figures (8 and 10), give four essential bands at (854nm, 11709cm^{-1}), (483nm, 20703cm^{-1}), (324nm, 30864 cm^{-1}), and (25nm, 39840cm^{-1}) for Rhodium (III) complex, whilst the bands of Platinum(IV) complex appeared at (848nm, 11792cm^{-1}), (520nm, 19230cm^{-1}), (387nm, 25839cm^{-1}), and (251nm, 39840 cm^{-1}) which attributed to the transitions $\nu_1={}^1A_1g\rightarrow$

^3T_1g, ^3T_1g, ν_2= $^1A_1g \rightarrow {}^1T_1g$, ν_3= $^1A_1g \rightarrow {}^1T_2g$, and ν_4=ILCT, respectively, and this corresponds to octahedral structure of both complexes [28,29].

Figures (9 and 11) show the spectrum of Pd(II) and Au(III) complexes and two main bands in the positions: (417nm, 23980cm^{-1}) and (381nm, 26246cm^{-1}) for Pd(II)-AL, while the bands of Au(III) complex present in (418nm, 23923cm^{-1}) and (308 nm, 32467cm^{-1}). The bands of these complexes ascribed to $^1A_1g \rightarrow {}^1B_1g$, $^1A_1g \rightarrow {}^1Eg$ respectively, which refers to the square planar geometry [7,29], in addition to the inter-ligand charge transfer (ILCT) transitions that exhibited between (200-277) nm as is clear in the mentioned figures.

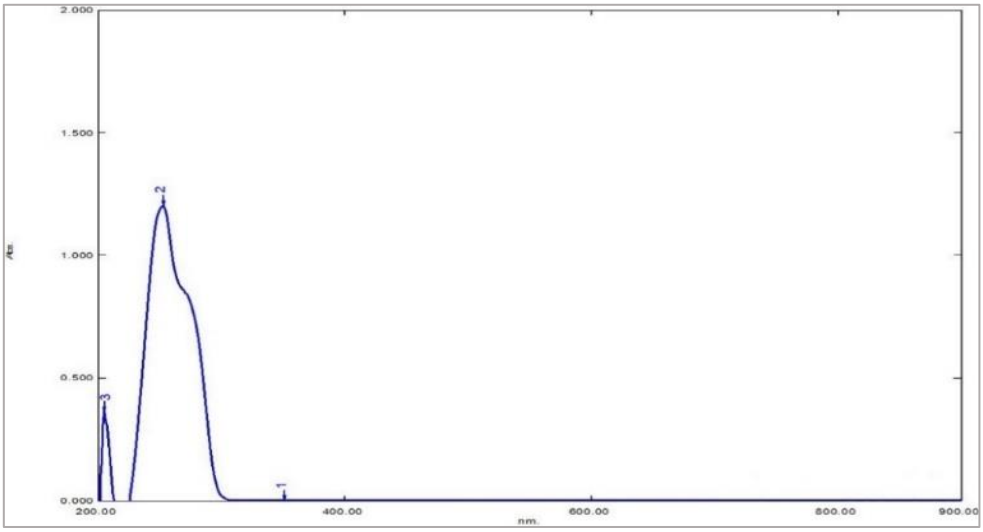

Figure 7: UV-Vis. spectrum of Acyclovir

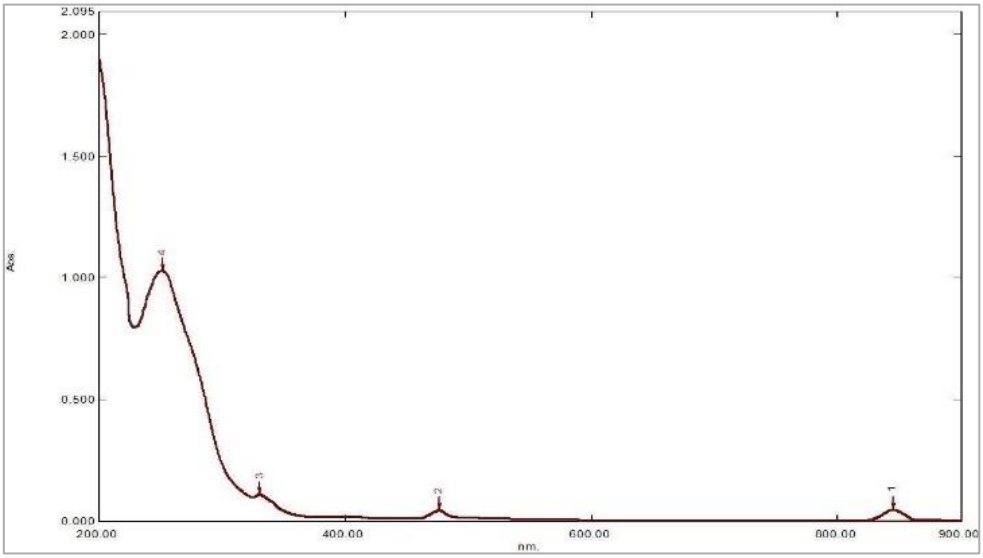

Figure 8: UV-Vis. spectrum of Rh-AL complex

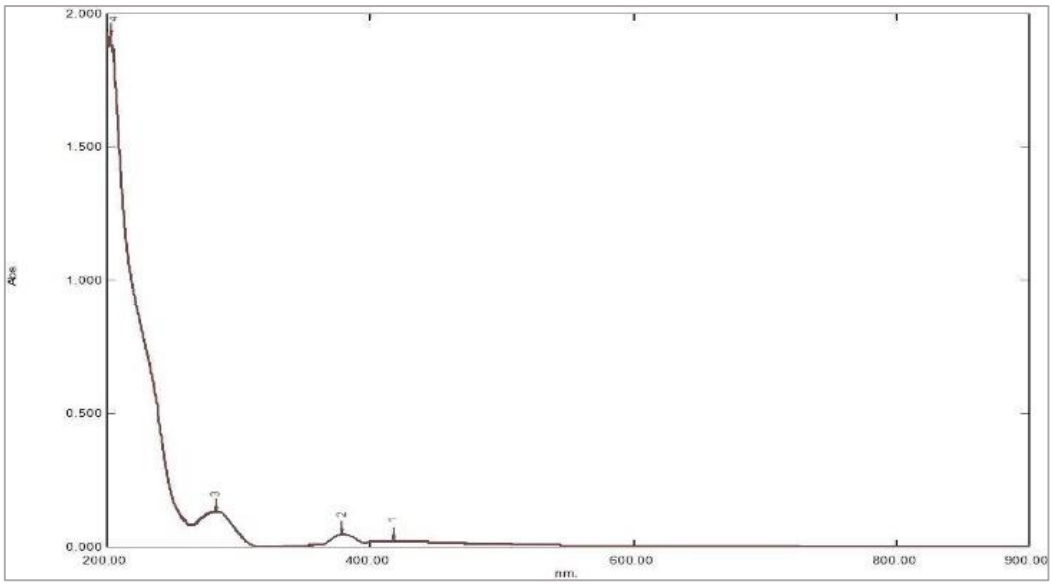

Figure 9: UV-Vis. spectrum of Pd-AL complex

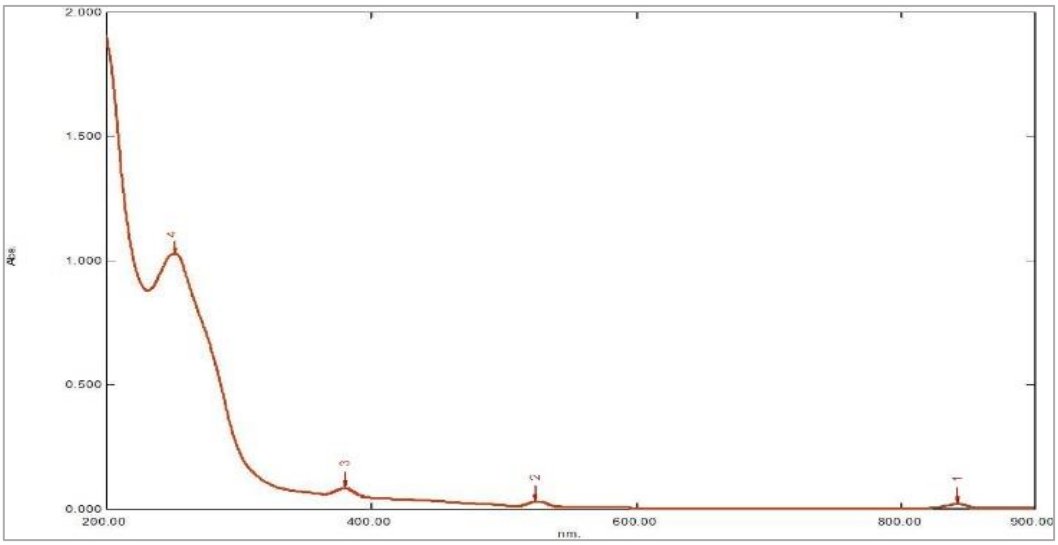

Figure 10: UV-Vis. spectrum of Pt-AL complex

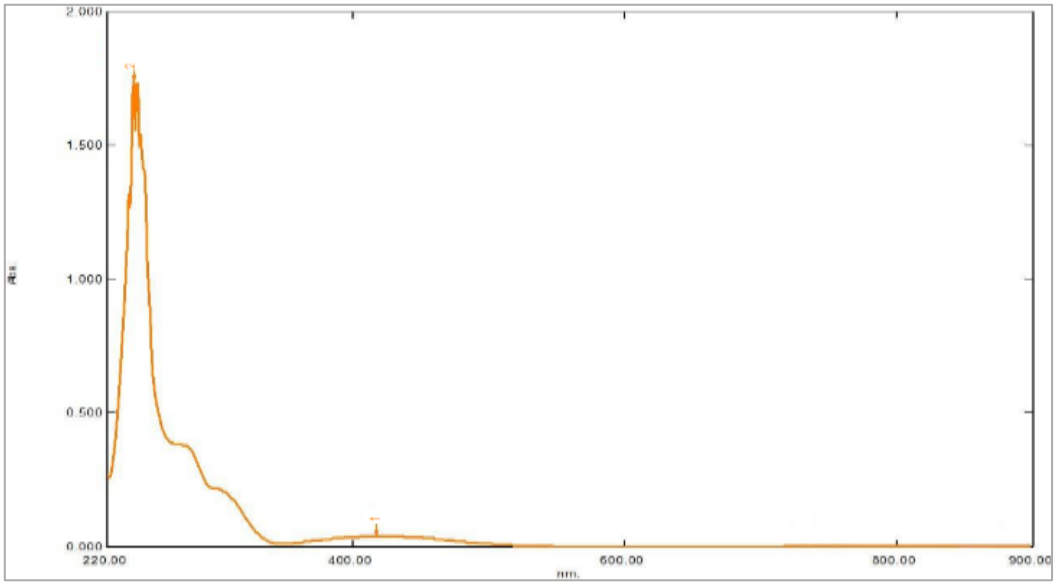

Figure 11: UV-Vis. spectrum of Au-AL complex

3.4-NMR Spectra of Au^{3+}-AL Complex

$^{1}H,^{13}C$-NMR spectra of $[Au(AL)_2]Cl_3.EtOH$ complex was studied and compared with spectral data of free Acyclovir molecules recorded in the study conducted by Hongwu and Ashim [30]. DMSO–d_6 has been used to obtain the spectral data for the studied complex. All the distinctive signals are summarized in Table 4 and Figures 12 and 13. In comparison, one can note the change in the value of chemical shifts in spectra of the complex, and this is due to the coordination of acyclovir with gold(III) ion and its effect on the shielding field, especially in the proton of imine group ($-HC^{8}=N^{7}-$) and carbon of carbonyl group $(C=O)^{6}$.

Table 4: Assigning the Au(III) complex and acyclovir according to NMR chemical shift (δ)/ppm

^{1}H-NMR			^{13}C-NMR			Structure
Proton	**AL**	**Au^{3+}-AL**	**Carbon**	**AL**	**Au^{3+}-AL**	
$-C^{12}H_2O-$	3.47	3.26	C^{13}	59.89	60.34	
$-C^{13}H_2O-$	3.47	3.26	C^{12}	70.38	70.81	
-OH	4.64	4.58	C^{10}	72.00	72.49	
$-NC^{10}H_2O-$	5.35	5.24	C^{8}	137.80	138.30/138.84	
$-NH_2$	6.52	6.41	C^{6}	156.80	157.33/159.84	
$-C^{8}H=N^{7}-$	7.82	7.46/7.45	C^{5}	116.37	116.85/118.23	
$-N^{1}H-$	10.67	10.54/10.94	C^{4}	151.40	151.12/151.88	
–	–	–	C^{2}	153.80	154.29	

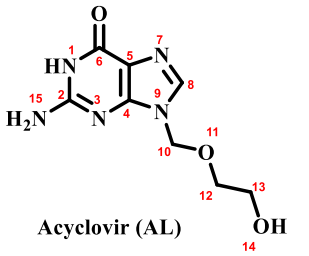

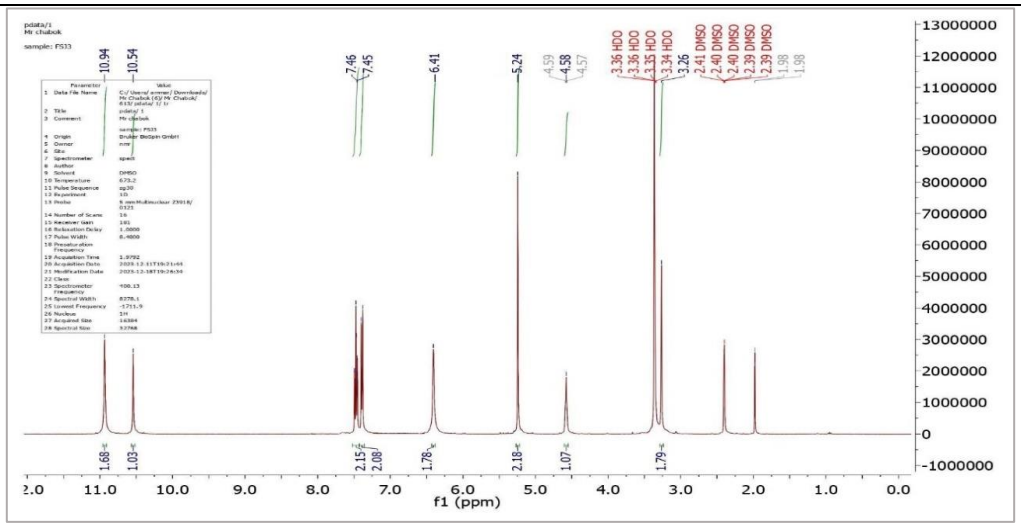

Figure 12: ^{1}H-NMR spectrum of Au^{3+}-AL Complex

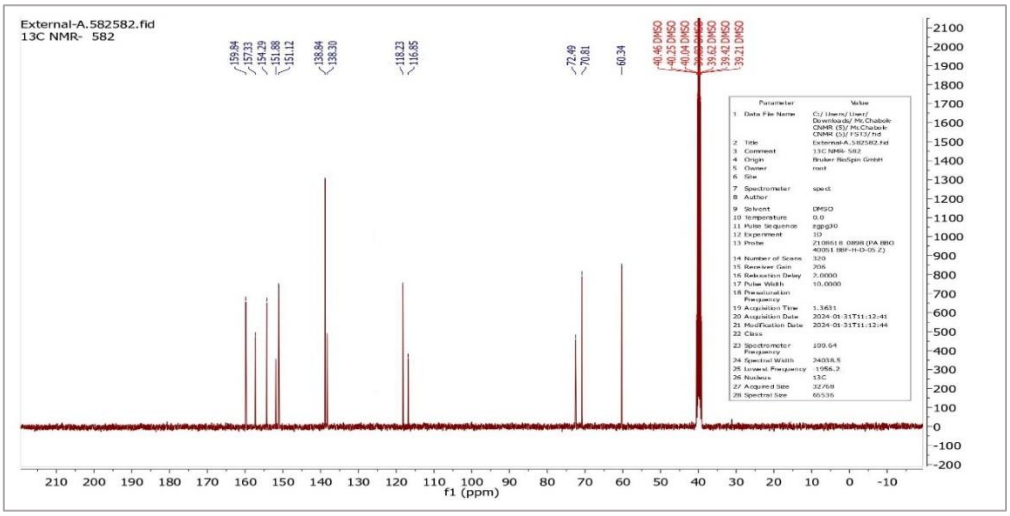

Figure 13: ^{13}C-NMR spectrum of Au^{3+}-AL Complex

3.5-Mass Spectrum of Au^{3+}-AL Complex

The mass spectrum and fragmentation pattern were carried out for the gold complex, as shown in Figure 14. The spectrum shows that the mass-to-charge ratio (m/z) of the parent peak is equal to 647.2, and this confirms the proposed molecular weight of Au(III)-complex ion (M.w = 647.38g/mol). The other fragment ions were assigned based on previous studies that deal with purines and their analogous [31].

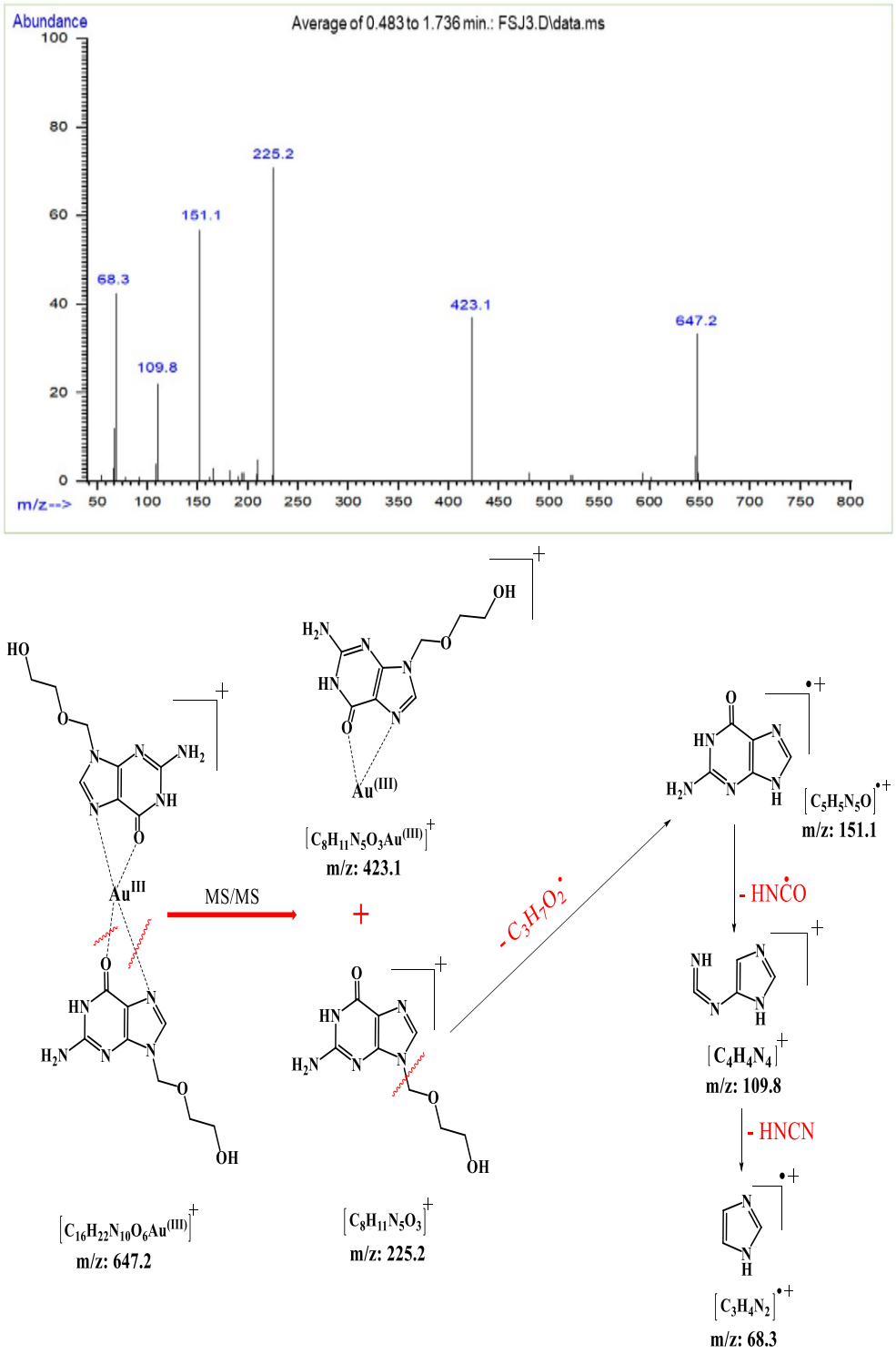

Figure 14: Mass spectrum and fragmentation pattern of Au^{3+}-AL Complex

Depending on the above spectral studies, the geometry of the prepared complexes is suggested in Figure 15.

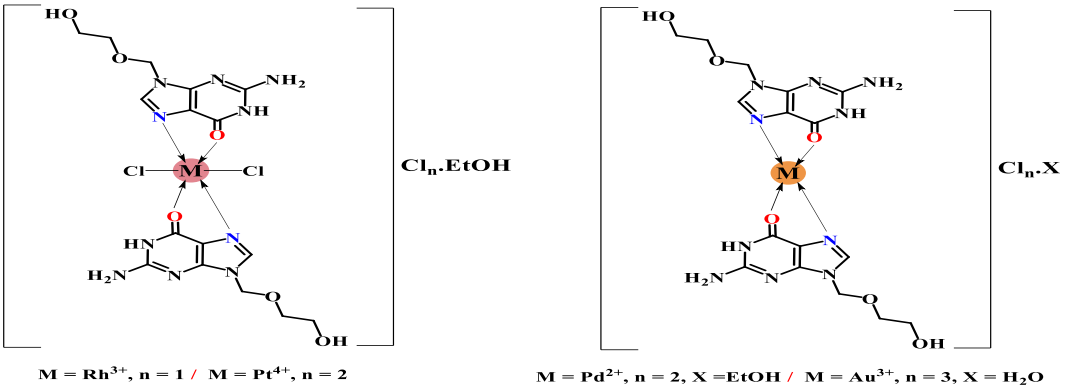

Figure 15: Proposed geometry of prepared complexes

3.6- Anticorrosive assay

3.6.1- Electrochemical measurement results

To determine the protection efficiencies of selected inhibitors (AL, Pt^{4+}-AL, and Au^{3+}-AL), the corrosion parameters involving the corrosion current densities (I_{corr} and $I_{corr(inh)}$), corrosion potentials (E_{corr}), and polarization resistance (Rp) for carbon steel (CS) specimen (in the absence and presence of inhibitors) were gained by extrapolation of cathodic and anodic Tafel curves (bc & ba) at 298K in 3.5(w/v) of NaCl solution, as shown in Table 5 and Figure 16(A-C). The values of polarization resistance (Rp), corrosion rate (CR), and percentage of corrosion inhibition (%IE) were calculated depending on the equations (7-9) [32], respectively.

$$Rp = \frac{ba \times bc}{2.303(ba+bc.)Icorr.} \quad \ldots \quad \text{Eq (7)}$$

$$CR = \frac{e}{\rho} \times 0.13 \times I_{corr.} \quad \ldots \quad \text{Eq (8)}$$

$$\%IE = \frac{I_{corr.} - I_{corr(inh)}}{I_{corr}} \times 100 \quad \ldots \quad \text{Eq (9)}$$

Where:

e = Chemical equivalent

ρ = Density of Carbon steel

$I_{corr.}$ = Corrosion current of blank carbon steel

$I_{corr(inh)}$ = Corrosion current of inhibitor-treated carbon steel. Note that in the case of treated carbon steel, it must be use $I_{corr(inh)}$ instead of I_{corr} in equations 7 and 8.

Table 5: Polarization data for carbon steel used before and after immersion with acyclovir or its complexes at various concentrations at 298 K in a 3.5% saline solution.

Inhibitor	Conc. (ppm)	-$E_{corr.}$ (mV)	$I_{corr.}$ (μA.cm^{-2})	-bc (mV/Dec)	ba (mV/Dec)	Rp (Ω.cm^2)	CR (g/m^2.d)	%IE
Blank	0.00	629.7	91.28	203.8	85.6	286.75	0.00	0.00
AL	20	712.1	2.84	58.9	105.0	5769.17	1.3117	96.89
	60	720.8	2.34	50.0	78.3	5662.33	1.0808	97.44
	80	704.5	1.44	51.4	45.5	7277.70	0.6651	98.42
Pt^{4+}–(AL)	20	582.4	4.34	163.4	83.8	5541.97	2.0045	95.25
	60	611.7	2.93	159.3	76.7	7672.51	1.3533	96.79
	80	652.0	2.58	123.0	56.3	6500.09	1.1916	97.17
Au^{3+}–(AL)	20	644.8	2.84	127.2	56.7	5996.20	1.3116	96.89
	60	657.7	1.81	97.6	62.5	9140.42	0.8359	98.02

	80	696.4	1.15	81.2	64.2	13537.39	0.5311	98.74

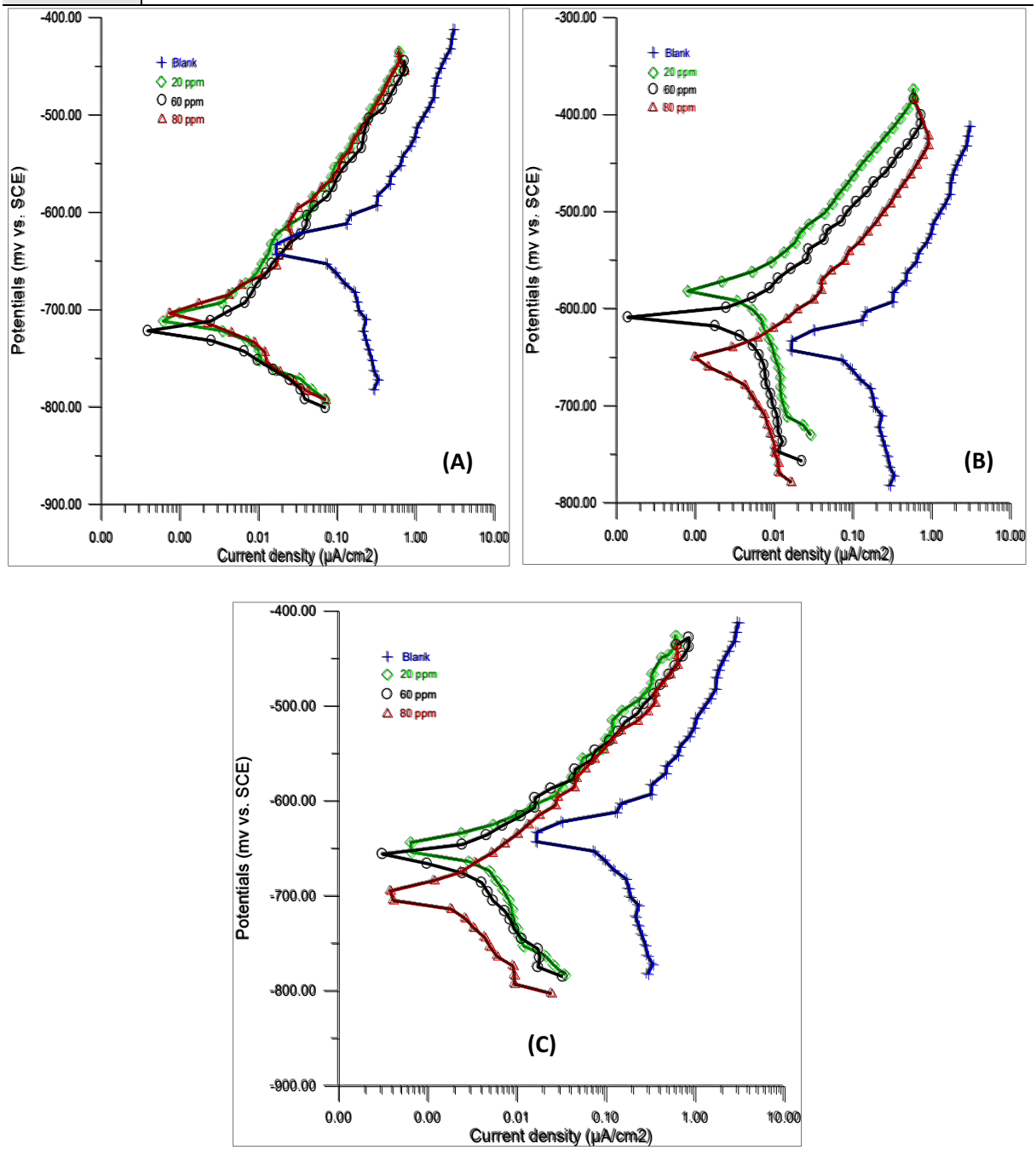

Figure 16: Tafel straight lines of carbon steel with different concentrations of (A): AL, (B): Pt^{4+}–(AL), and (C): Au^{3+}–(AL) in 3.5 % NaCl at 25°C.

From the results shown in Table 5, one can observe that the corrosion rate decreases with increasing concentrations of inhibitors, which belongs to an increase in the adsorption of inhibitors on the surface of carbon steel specimens. Generally, the results show high inhibition efficiency values for all tested compounds and can be considered mixed-type inhibitors because both anodic and cathodic reactions were impacted. By comparing this study with the work that was conducted by Chandrabhan *et al.,*[33], which included examining the capability of acyclovir to inhibit the corrosion rate of mild steel in an acidic medium (0.1M HCl) by electrochemical and gravimetric methods. It was found that acyclovir gave high IE% reached 92% at 500 ppm, while a higher inhibition efficiency = 98.42% was

obtained at a lower concentration equal to 80 ppm, considering the variation in the corrosive environment. The potential of acyclovir and its complexes to inhibit the rate of corrosion can be attributed to several factors, including the presence of π-electrons and lone pair of electrons in the structure of ligand that can interact with the metal in CS specimen[34], also the charges of atoms/ species can cause electrostatic attraction/ repulsion forces with charged of metals on the surface of specimen and this may explain the potential of complexes for inhibition of corrosion[35].

3.6.2- The Surface Morphology of CS specimen

The images of SEM Figure 17 show the participants (absorbed) the particles of inhibitors on the surface of carbon steel. These particles formed a barrier layer between corrosive media and the surface of CS [36].

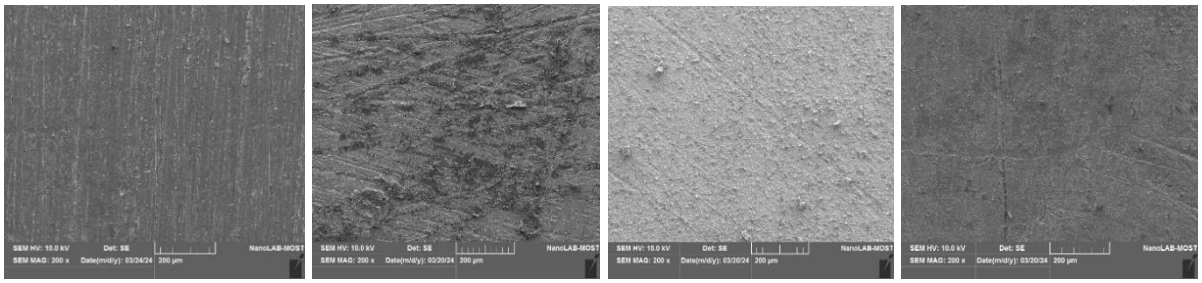

A B C D

Figure 17: SEM of corroded CS plate at 200μm (A) in the absence of inhibitor, in the presence of one of the inhibitors: (B) AL, (C) Pt^{4+}-AL, and (D) Au^{3+}-AL.

3.7- Antibiofilm Activity of Acyclovir and Its complexes

In this work, the inhibition of biofilm produced by the isolates of Gram-negative bacterium *E. coli* on a hydrophobic surface was studied by acyclovir and its complexes and compared with negative control. The study included testing the compounds in sub-MIC concentration, and here, it must be mentioned that the sub-MICs are different for each compound. Practically, it was found that sub-MIC for tested compounds is as follows: (AL = 512, Rh^{3+}–AL = 32, Pd^{2+}–AL = 256, Pt^{4+}–AL = 256, Au^{3+}–AL = 128) in (μg/ml). All tested compounds showed the capability to prevent microbial adhesion by more than 50% at these concentrations, as shown in Table 6 and Figure 18. The rhodium(III) complex can be considered the most effective relative to other compounds, as it exhibited I%= 56.43% at 32μg/ml, followed by Au^{3+}–AL which showed I%= 60.52% at 128μg/ml (i.e. four times the concentration of Rh^{3+}-AL), and this may be attributed to the oxidation state of both metals that lead to increases membrane damage and prevents quorum sensing (cell-cell communication system of bacteria)[37].

Table 6: The percentage of biofilm inhibition of treated *E coli* isolate with sub-MIC of Acyclovir and Its complexes

Compounds	sub-MIC	Mean of OD_{630} ± SD	I%
Control	-	0.733 ± 0.018	0.00
AL	512	0.297 ± 0.0757	59.48
Rh-AL	32	0.319 ± 0.0466	56.43
Pd-AL	256	0.347 ± 0.0430	52.61
Pt-AL	256	0.319 ± 0.0476	56.48
Au-AL	128	0.289 ± 0.0456	60.52

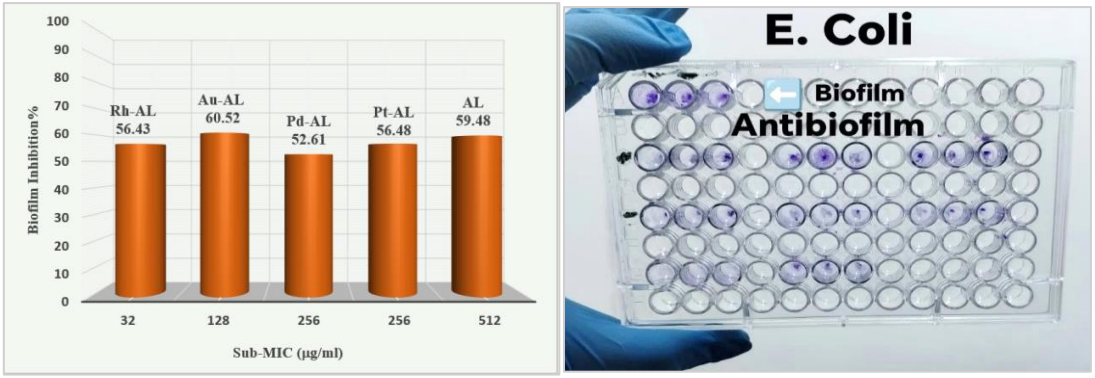

Figure 18: Right: 96-well microplate of antibiofilm test, Left: effect of sub-MIC of acyclovir and its complexes on the biofilm formation.

3.8- Antioxidant Activity of Acyclovir and Its complexes

The antioxidant property of acyclovir and its prepared complexes was determined according to the popular and easy DPPH method. The findings presented high scavenging capacity by acyclovir and some complexes compared with ascorbic acid, as shown in Figure 19. In general, the tested compounds can be arranged according to their effectiveness at high concentrations as follows: Rh^{3+}–AL > AL > Pt^{4+}–AL > Au^{3+}–AL > Pd^{2+}–AL. The ability to scavenge DPPH free radicals is due to the -OH group of acyclovir ligand, besides the impact of Rh(III) and Pt(IV) ions to increase the electron-withdrawing from the amide group (-NH-CO-) makes it more acidic [38]. Also, the Oh geometry of Rh(III) and Pt(IV) complexes supports them by maintaining their stability during the scavenging process[39]. The mean results for each complex at each concentration, as well as the IC50 values, are shown in Table 7.

Table 7: The antioxidant activity of acyclovir and its complexes according to the DPPH approach

Compounds	Concentration (µg/ml)					Linear eq	R^2	IC_{50} (µg/ml)
	12.5	25	50	100	200			
Ascorbic acid	36.23	54.67	64.27	74.07	79.7	y = 0.1909x + 46.997	0.7166	15.73
AL	39.85	55.75	63.66	73.07	78.97	y = 0.1742x + 48.76	0.7485	7.11
Rh-AL	40.59	52.05	66.05	74.54	81.56	y = 0.1927x + 48.022	0.7787	10.26
Pd-AL	13.39	13.93	17.21	27.04	32.1	y = 0.1061x + 12.515	0.9286	353.29
Pt-AL	42.4	53.05	65.16	71.22	76.16	y = 0.1548x + 49.601	0.7341	2.57
Au-AL	16.51	31.67	41.13	53.97	63.81	y = 0.2221x + 24.204	0.8345	116.14

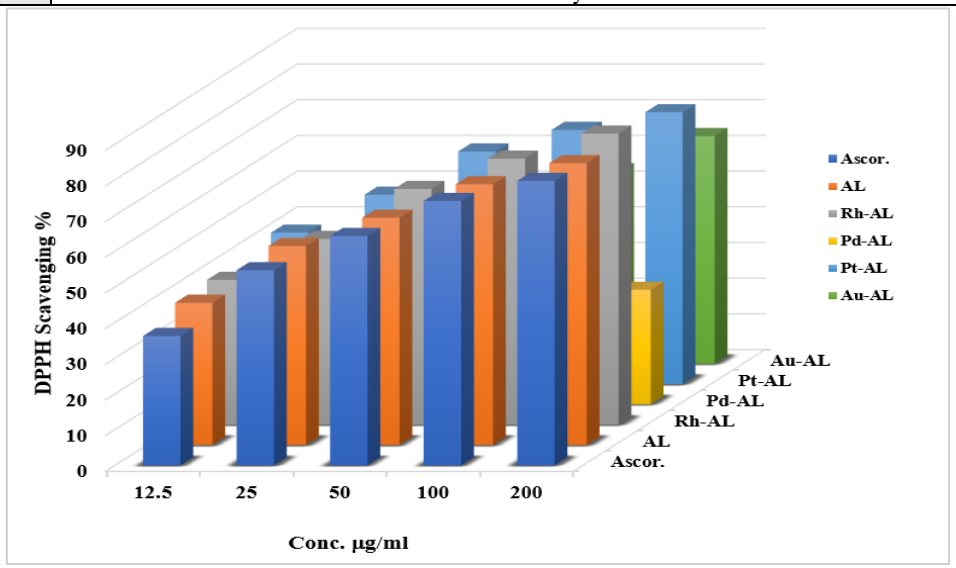

Figure 19: Bar chart of DPPH Scavenging efficiency of acyclovir and its complexes

3.9-Antiproliferative Activity of Acyclovir and some complexes

Acyclovir and its complexes of Pt(IV) and Au(III) were used to study cell viability against human foreskin fibroblasts (HFFs) cancer cell lines at different concentrations for 72 hours, and all results are collected in Table 8. All compounds show the ability to reduce the proliferation of cancer cells at high concentrations. However, the gold (III) complex was more influential than others, as it showed antiproliferative activity at all tested concentrations. Meanwhile, the results for the acyclovir and Pt(IV) complex varied depending on the concentration used. So, the activity of Au(III) may be due to specifically targeting cancer cells by causing the production of reactive oxygen species, which damages DNA and causes cell death [40]. Figures 20 and 21 showed the viability against concentration and the morphology of cells, respectively.

Table 8: Antiproliferative assay results of Acyclovir and Pt(IV) & Au(III)complexes vs. HFFs cancer cell line

Comp.	Conc. (µg/ml)	OD_{540nm} ± SD	Viability%	Linear eq	R^2	IC_{50} (µg/ml)
Control	-	471.25 ± 19.189	100	-	-	-
AL	12.5	466.5 ±5.802	98.99	y = -0.0717x + 97.082	0.8468	671.42
	25	471.75 ± 14.773	100			
	50	411 ± 1.414	87.21			
	100	397.5 ± 5.686	84.35			
	200	385.25 ±10.50	81.75			
	400	333 ± 6.733	70.663			
Pt-AL	12.5	481 ± 8.286	102.69	y = -0.0884x + 100.52	0.9414	625
	25	479.25 ± 13.475	101			
	50	453 ± 6.218	96.12			
	100	411.25 ± 14.863	87.26			
	200	372.25 ± 15.129	78.99			
	400	320 ± 6.976	67.90			
Au-AL	12.5	456.25 ± 4.645	96.81	y = -0.072x + 93.481	0.832	621.14
	25	424.75 ± 6.396	90.13			
	50	402 ± 7.164	85.30			
	100	386.75 ± 10.904	82.06			
	200	353.75 ± 17.670	75.06			
	400	321.75 ± 9.742	68.27			

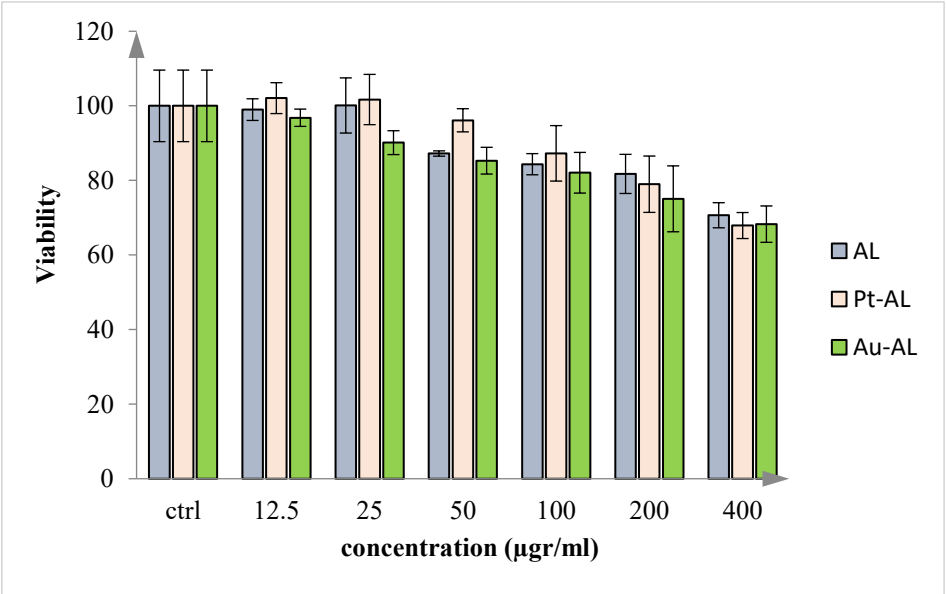

Figure 20: Different concentrations of acyclovir and its complexes affect the viability of HFFs cells

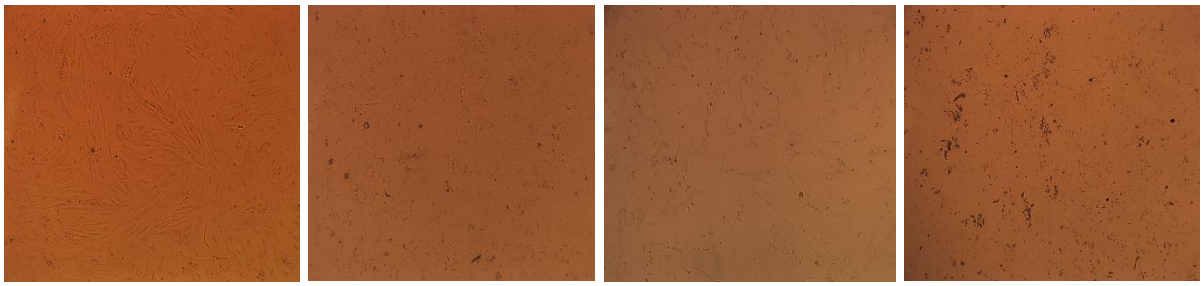

A B C D

Figure 21: Morphological changes of the control sample (A) after being treated separately with AL (B), Pt-AL (C), and Au-AL, respectively.

4. Conclusion

Four new metal-organic complexes in (1:2) molar ratios were synthesized from acyclovir drug and characterized by several techniques. All obtained spectral and analysis data indicate the bidentate behaviour of Acyclovir (AL) from O^6, N^7-donor atoms. The coordination shape of synthesized complexes is divided into square planar geometry for Pd(II) and Au(III) complexes and octahedral for Rh(III) and Pt(IV) complexes.

These complexes with ligand (AL) have undergone some applications to evaluate their performance in inhibiting corrosion, inhibiting biofilm formation, scavenging DPPH free radicals, and inhibiting cancer cell proliferation. These applications have been done in different concentrations. In general, the efficiency of compounds increases at high concentrations. Therefore, the classification of the effectiveness of compounds for each application can be summarized as follows: Au^{3+}–AL is greater than AL and AL was more effective than Pt^{4+}–AL (as anticorrosive at 80ppm vs. CS specimen in saline solution), while Rh^{3+}–AL is greater than AL and AL is much more effective than Pt^{4+}–AL which is shown a higher efficiency than Au^{3+}–AL and the later was more than Pd^{2+}–AL (as an antioxidant at 200µg/ml vs. DPPH free radicals), and Au^{3+}–AL was shown a high efficiency than Pt^{4+}–AL and the rest was more than AL (as antiproliferative at 200µg/ml vs. HFFs cancer cells). With respect to antibiofilm activity against *E coli* using the sub-MIC for each compound, the results showed that Rh^{3+}–AL is the most effective and can inhibit 56.43% of biofilm formation at 32µg/ml, while other compounds required a higher concentration to get the same results.

Acknowledgements

The authors are greatly obliged to the administration of the Department of Chemistry, College of Science for Women, University of Baghdad, Iraq to provide the opportunity to complete some parts of this work within its laboratories.

Conflict of Interest

The authors declare that they have no conflicts of interest.

References

[1] A. Majewska and B. Mlynarczyk-Bonikowska, "40 years after the registration of acyclovir: do we need new anti-herpetic drugs?, " *International journal of molecular sciences,* vol. 23, no. 7, pp. 1-33, 2022. https://doi.org/10.3390/ijms23073431.

[2] S. Kausar, F. Said-Khan, M. R. Ishaq., M. Akram, M. Riaz, G. Rasool, A. Hamid-Khan, I. Saleem, S. Shamim and A. Malik "A review: Mechanism of action of antiviral drugs," *International journal of immunopathology and pharmacology,* vol. 35, pp. 1-12, 2021. https://doi.org/10.1177/20587384211002621.

[3] K. Shiraki, M. Takemoto and T. Daikoku, "Emergence of varicella-zoster virus resistance to acyclovir: epidemiology, prevention, and treatment," *Expert review of anti-infective therapy* vol. 19, no. 11, pp. 1415-25, 2021. https://doi.org/10.1080/14787210.2021.1917992.

[4] H. H. Schalkwijk, R. Snoeck and G. Andrei, "Acyclovir resistance in herpes simplex viruses: Prevalence and therapeutic alternatives," *Biochemical Pharmacology,* vol. 206, pp. 1-12, 2022. https://doi.org/10.1016/j.bcp.2022.115322.

[5] F. Picarazzi and M. Mori, *Chapter 2.1DNA and RNA polymerases. InMetalloenzymes, Academic Press,* 2024, p. 9-22. https://doi.org/10.1016/B978-0-12-823974-2.00011-5.

[6] A. Birkmann, S. Bonsmann, D. Kropeit, T. Pfaff, M. Rangaraju, M. Sumner, B. Timmler, H. Zimmermann, H. Buschmann and H. Ruebsamen-Schaeff, "Discovery, chemistry, and preclinical development of pritelivir, a novel treatment option for acyclovir-resistant herpes simplex virus infections," *Journal of Medicinal Chemistry*, vol. 65, no. 20, pp. 13614-28, 2022. https://pubs.acs.org/doi/full/10.1021/acs.jmedchem.2c00668.

[7] F. S. Jaafar and M. F. Alias "Chemistry of Metalloguanines: An Overview of Their Synthesis Routes and Their Implementations for the Period 2000-2024," *Karbala International Journal of Modern Science*, vol. 11, no. 1, pp. 1-12, 2025. https://doi.org/10.33640/2405-609X.3392.

[8] E. Boros, P. J. Dyson and G. Gasser, "Classification of metal-based drugs according to their mechanisms of action," *Chem*, vol. 6, no. 1, pp. 41-60, 2020. https://doi.org/10.1016/j.chempr.2019.10.013.

[9] B. Blažič, I. Turel, N. Bukovec, P. Bukovec and F. Lazarini, "Synthesis and structure of diaquadichlorobis {9-[(2-hydroxyethoxy) methyl] guanine} copper (II)," *Journal of inorganic biochemistry*. vol. 51, no. 4, pp. 737-44,1993. https://doi.org/10.1016/0162-0134(93)85006-T.

[10] M. Panteva, T. Varadinova and I. Turel, "Effect of Copper Acyclovir Complexes on Herpes Simplex Virus Type 1 and Type 2 (HSV-1, HSV-2) Infection in Cultured Cells," *Metal-Based Drugs,* vol. 5, no. 1, pp. 19-23,1998. https://doi.org/10.1155/MBD.1998.19.

[11] P. B. María del, Ch.-L. Duane, D.-M. Alicia, J. M. González-Pérez, C. Alfonso and J. Niclós-Gutiérrez, "Metal ion binding patterns of acyclovir: Molecular recognition between this antiviral agent and copper (II) chelates with iminodiacetate or glycylglycinate," *Journal of Inorganic Biochemistry,* vol. 105, no. 5, pp. 616-23, 2011. https://doi.org/10.1016/j.jinorgbio.2011.02.001.

[12] A. Sinur and S. Grabner, "A platinum (II) diammine complex: cis-[Pt $(C_8H_{11}N_5O_3)_2(NH_3)_2]Cl_2.2H_2O$," *Acta Crystallographica Section C: Crystal Structure Communications,* vol. 51, no. 9, pp. 1769-72,1995. https://doi.org/10.1107/S0108270195002563.

[13] M. Coluccia, A. Boccarelli, C. Cermelli, M. Portolani and G. Natile, "Platinum (II)-Acyclovir Complexes: Synthesis, Antiviral and Antitumour Activity," *Metal-Based Drugs,* vol. 2, no. 5, pp. 249-56, 1995. https://doi.org/10.1155/MBD.1995.249.

[14] Z. Balcarová, J. Kaspárková, A. Zákovská, O. Nováková, M. F. Sivo, G. Natile and V. Brabec, "DNA interactions of a novel platinum drug, cis-[PtCl $(NH_3)_2$(N7-Acyclovir)]$^+$," *Molecular pharmacology*, vol. 53, no. 5, pp. 846-55, 1998. https://molpharm.aspetjournals.org/content/53/5/846.

[15] J. Gómez-Segura, S. Caballero, V. Moreno, M. J. Prieto and A. Bosch, "Palladium (II) binding to N (7) of acyclovir: DNA interaction and herpes simplex virus (HSV-1) inhibitory activity," *Journal of inorganic biochemistry,* vol. 103, no. 1, pp. 128-34, 2009. https://doi.org/10.1016/j.jinorgbio.2008.09.018.

[16] Á. García-Raso, J. J. Fiol, F. Bádenas, R. Cons, Á. Terrón and M. Quirós, "Synthesis and structural characteristics of metal–acyclovir (ACV) complexes: [Ni (or Co) $(ACV)_2(H_2O)_4]Cl_2 \cdot 2ACV$, $[Zn(ACV)Cl_2(H_2O)]$,[Cd $(ACV)Cl_2]\cdot H_2O$ and [{$Hg(ACV)Cl_2$}x]. Recognition of acyclovir by Ni–ACV, " *Journal of the Chemical Society, Dalton Transactions,* no. 2, pp. 167-74, 1999. https://doi.org/10.1039/A807787H.

[17] T. Varadinova, N. Vilhelmova, F. Badenas, A. Terron, J. Fiol, A. Garcia-Raso and P. Genova, "Effect of metal complexes of acyclovir and its acetylated derivative on Herpes simplex virus 1

and Herpes simplex virus 2 replication. Acta virologica," vol. 49, no. 4, pp. 251, 2005. https://pubmed.ncbi.nlm.nih.gov/16402682/.

[18] A. M. Vahdettin and A. Golcu, "Synthesis of acyclovir metal complexes: Spectral, electrochemical, thermal, and DNA binding studies," *Synthesis and Reactivity in Inorganic, Metal-Organic, and Nano-Metal Chemistry,* vol. 45, no. 4, pp. 581-590, 2015. https://doi.org/10.1080/15533174.2013.831877.

[19] M. A. El-ghamry, K. M Nassir, F. M. Elzawawi, A. A. Aziz and S. M. Abu-El-Wafa, "Novel nanoparticle-size metal complexes derived from acyclovir. Spectroscopic characterization, thermal analysis, antitumor screening, and DNA cleavage, as well as 3D modeling, docking, and electrical conductivity studies," *Journal of Molecular Structure*, vol. 1235, no. 130235, pp. 1-17, 2021. https://doi.org/10.1016/j.molstruc.2021.130235.

[20] F. R. Mansour and N. D. Danielson, "Ligand exchange spectrophotometric method for the determination of mole ratio in metal complexes, " *Microchemical Journal*, vol. 1, no. 103, pp. 74-78, 2012. https://doi.org/10.1016/j.microc.2012.01.008.

[21] I. M. Al-mousawi, R. S. Ahmed, N. J. Kadhim and A. M. Farhan, "Study of Corrosion Inhibition for Mild Steel in Hydrochloric Acid Solution by a new furan derivative," *InJournal of Physics: Conference Series* vol. 1879, no. 2, pp. 1-10, 2021 https://doi:10.1088/1742-6596/1879/2/022061.

[22] S. Wang, H. Wang, B. Ren, H. Li, M. D. Weir, X. Zhou, T. W. Oates, L. Cheng and H. H. Xu, "Do quaternary ammonium monomers induce drug resistance in cariogenic, endodontic and periodontal bacterial species?," *Dental Materials*, vol. 33, no. 10, pp. 1127-1138, 2017. https://doi.org/10.1016/j.dental.2017.07.001.

[23] S. Baliyan, R. Mukherjee, A. Priyadarshini, A. Vibhuti, A. Gupta, R. P. Pandey and C. M. Chang "Determination of antioxidants by DPPH radical scavenging activity and quantitative phytochemical analysis of Ficus religiosa," *Molecules*, vol. 27, no. 4, pp. 1-19, 2022. https://doi.org/10.3390/molecules27041326.

[24] F. I. Abdullaev, L. Riveron-Negrete, H. Caballero-Ortega, J. M. Hernández, I. Perez-Lopez, R. Pereda-Miranda and J. J. Espinosa-Aguirre, "Use of in vitro assays to assess the potential antigenotoxic and cytotoxic effects of saffron (Crocus sativus L.)," *Toxicology in vitro*, vol.17, no. 5-6, pp. 731-736, 2003. https://doi.org/10.1016/S0887-2333(03)00098-5.

[25] P. Zaby, J. Blasius, AK. Müller, SP. Nolan and O. Hollóczki "Liquid Dynamics Determine Transition Metal-N-Heterocyclic Carbene Complex Formation, " *Chemistry–A European Journal*, vol. 29, no. 18, pp.1-9, 2023. https://doi.org/10.1002/chem.202203636.

[26] B. H. Stuart, *Infrared spectroscopy: fundamentals and applications. John Wiley & Sons*, 2004. https://onlinelibrary.wiley.com/doi/book/10.1002/0470011149

[27] M. G. Abd El-Wahed, M. S. Refat and S. M. El-Megharbel, "Metal complexes of antiuralethic drug: synthesis, spectroscopic characterization and thermal study on allopurinol complexes," *Journal of Molecular Structure,* vol. 888, no. 1-3, pp. 416-429, 2008. https://doi.org/10.1016/j.molstruc.2008.01.009.

[28] S. J. Swamy, B. V. Pratap, P. Someshwar, K. Suresh and D. Nagaraju, "Synthesis and spectral studies of Iron (III), ruthenium (III) and Rhodium (III) complexes with new tetraaza macrocyclic ligands," *Journal of Chemical Research,* vol. 2005, no. 5, pp. 313-315, 2005. https://doi.org/10.3184/0308234054323986.

[29] M. D. Radovanović, M. S. Ristić, M. Zlatar, F. W. Heinemann and Z. D. Matović, "New rhodium (III)–ED3AP complex: Crystal structure, characterization and computational chemistry," *Journal of the Serbian Chemical Society,* vol. 87, no. 5, pp. 561-573, 2022. http://dx.doi.org/10.2298/JSC211230003R.

[30] H. Gao and A. K. Mitra, "NMR spectral data for acyclovir prodrugs, "*Magnetic resonance in chemistry,* vol. 37, no. 9, pp. 687-689, 1999. https://doi.org/10.1002/(SICI)1097-458X(199909)37:9%3C687::AID-MRC510%3E3.0.CO;2-K.

[31] M. A. El-Ghamry, F. M. Elzawawi, A. A. Aziz, K. M. Nassir and S. M. Abu-El-Wafa, "New Schiff base ligand and its novel Cr (III), Mn (II), Co (II), Ni (II), Cu (II), Zn (II) complexes: spectral investigation, biological applications, and semiconducting properties," *Scientific Reports,* vol. 12, no. 17942, pp. 1-22, 2022. https://www.nature.com/articles/s41598-022-22713-z.

[32] R. A. Jasim, N. J. Kadhim, A. M. Farhan and M. S. Hadi, "Nano-Parctials as corrosion inhibitors for Aluminum alloys in acidic solution at different Temperatures," *InIOP Conference Series: Materials Science and Engineering,* vol. 928, no. 5, pp. 1-11, 2020. https://iopscience.iop.org/article/10.1088/1757-899X/928/5/052014/meta.

[33] C. Verma, M. A. Quraishi and E. E. Ebenso, "Electrochemical studies of 2-amino-1, 9-dihydro-9-((2-hydroxyethoxy) methyl)-6H-purin-6-one as green corrosion inhibitor for mild steel in 1.0 M hydrochloric acid solution," *International Journal of Electrochemical Science,* vol. 8, no. 5, pp. 7401-7413, 2013. https://doi.org/10.1016/j.tsf.2023.140005.

[34] L. Huang, W. Liu, J. Shen and Q. Liao, "Study of antiviral drug Famciclovir as a corrosion inhibitor for carbon steel in hydrochloric acid medium," *Thin Solid Films,* vol. 782, pp. 1-14, 2023. https://doi.org/10.1016/j.tsf.2023.140005

[35] A. Chaouiki, M. Chafiq, Y. G. Ko, A. H. Al-Moubaraki, F. Z. Thari, R. Salghi, K. Karrouchi, K. Bougrin, I. H. Ali and H. Lgaz, "Adsorption mechanism of eco-friendly corrosion inhibitors for exceptional corrosion protection of carbon steel: electrochemical and first-principles DFT evaluations," *Metals,* vol. 12, no. 10, pp.1-20, 2022. https://doi.org/10.3390/met12101598.

[36] H. Wang, S. Sharma, A. Pailleret, B. Brown and S. Nešić, "Investigation of corrosion inhibitor adsorption on mica and mild steel using electrochemical atomic force microscopy and molecular simulations," *Corrosion,* vol.78, no. 10, pp. 990-1002, 2022. https://doi.org/10.5006/4136.

[37] P. Shree, C. K. Singh, K. K. Sodhi, J. N. Surya and D. K. Singh, "Biofilms: Understanding the structure and contribution towards bacterial resistance in antibiotics," *Medicine in Microecology,* vol. 16, pp. 1-11, 2023. https://doi.org/10.1016/j.medmic.2023.100084

[38] T. M. Asha and M. R. Prathapachandra-Kurup, "An insight into the potent antioxidant activity of a dithiocarbohydrazone appended cis-dioxidomolybdenum (VI) complexes," *Applied Organometallic Chemistry,* vol. 34, no. 9, pp. 1-14, 2020. https://doi.org/10.1002/aoc.5762.

[39] H. M. El-Lateef, T. El-Dabea, M. M. Khalaf and A. M. Abu-Dief, "Recent overview of potent antioxidant activity of coordination compounds," *Antioxidants,* vol. 12, no. 2, pp. 1-36, 2023. https://doi.org/10.3390%2Fantiox12020213.

[40] A. Alhoshani, A. A. Sulaiman, H. M. Sobeai, W. Qamar, M. Alotaibi, K. Alhazzani, M. Monim-ul-Mehboob, S. Ahmad and A. A. Isab, "Anticancer activity and apoptosis induction of gold (III) complexes containing 2, 2′-bipyridine-3, 3′-dicarboxylic acid and dithiocarbamates," *Molecules,* vol. 26, no. 13, pp. 1-16, 2021. https://doi.org/10.3390%2Fmolecules26133973.ش